Uniaxial Dynamic Compressive Properties of HTPB Casting Explosives

Youcai Xiao[1]*, Yi Sun[2], Zhijun Wang[1], Zhongsi Xu[1], Tiexiong Su[1]

[1] College of Mechatronic Engineering, North University of China, Taiyuan 030051, China

[2] Department of Astronautic Science and Mechanics, Harbin Institute of Technology, Harbin 150001, China

Corresponding author: Youcai Xiao (x_youcai@163.com)

ABSTRACT The dynamic mechanical properties of hydroxy-terminated polybutadiene (HTPB) casting explosives were investigated using the split Hopkinson bar technique. Based on the split Hopkinson pressure bar technique, the thickness of the specimen and the shape of the incident wave are designed to ensure the rationality of the experimental results. Based on a strain energy function theory, a one-dimensional constitutive relation was developed to describe the dynamic mechanical behavior of explosive.

KEYWORD: Polymer bonded explosives; Split Hopkinson pressure bar; Dynamic stress uniformity; Constitutive relations

Introduction

Polymer bonded explosives (PBXs) have usually been considered as a particulate composite material containing the energetic grains embedded in a polymeric binder [1-6]. Compared with low binder content PBXs (such as PBX9501, PBX9502, EDC37), cast-cured explosives (e.g., PBXN-109, PBXN-110, LX-10) are easier to fill into micro

and complex structures due to their better flow characteristics. The dynamic mechanical property of PBXs is strongly influenced by strain rates and temperatures [7-10].

The split Hopkinson pressure bar (SHPB), originally developed by Kolsky [11], has been widely used and modified to determine the dynamic properties of a variety of engineering materials, such as metals and concrete. Chen et al. [12-17] pointed out that the modified conventional SHPB can be used for testing the compressive stress-strain curves of materials with low mechanical impedance and low compressive strengths, such as a silicone and polyurethane foam. Chen and Lu et al. [18] found that the thickness of specimens and the incident wave are very critical for the rationality of result with soft materials in SHPB tests. Frew et al. [19, 20] studied the pulse shaping techniques for testing brittle materials in a SHPB. In their paper, they presented an analytical model and data, which indicated that a wide variety of incident waves can be produced by varying the geometry and the length of the copper disks. Frantz et al. wrote a review paper that discussed the pulse shaper for SHPB experiments with metal sample. In the review paper, the authors emphasized that the pulse shaper technique can minimize the effects of dispersion, and the specimen can achieve dynamic stress equilibrium. In addition, Follansbee et al. [21] showed that the pulse shaper can be used to generate a nearly constant strain rate in the specimen. Duffy et al. [22] used pulse shapers to smooth pulses generated by explosive loading for the torsional split Hopkinson bar. High binder content PBXs is a kind of soft materials, so the mechanical impedance is lower than that of metals as well as concrete and so on.

Low-strength and low-impedance materials pose significant challenges in the design of experiments to determine dynamic stress-strain curves.

A number of constitutive relations have been developed to model the mechanical behavior of polymers [23-25]. Most constitutive relations have been aimed at different aspects of these observations, such as infinitesimal deformation, strain rates, temperatures, and the yield phenomenon. Each of these approaches has its advantages, but it still appears that a constitutive relation for the tensile behavior of PBX is not readily available. A significant factor is the difficulty of determining the parameters required for the various models.

In this research, a modified SHPB setup was conducted to study the dynamic mechanical behavior of PBX. Dynamic compressive stress-strain curves were obtained under valid experimental conditions. Based on the strain-energy function theory, a constitutive relation was developed to model the dynamic mechanical behavior of PBX.

Experimental details

Materials

The PBX is a heterogeneous material of 60 wt. % energetic RDX grains embedded in 40 wt. % polymer binder. The polymer binder is composed of a plasticizer, a curing catalyst, a reactant and nanometric aluminum powder. The sizes of RDX are about 50 μm ~ 200 μm. The density is 1.69 g/cm3. The scanning electron microscope (SEM Helios Nanolab 600i) of PBX specimens is shown in Fig. 1. Here, a pristine sample of PBX shows distribution of RDX grains, and the micrograph is from a cut cross-section.

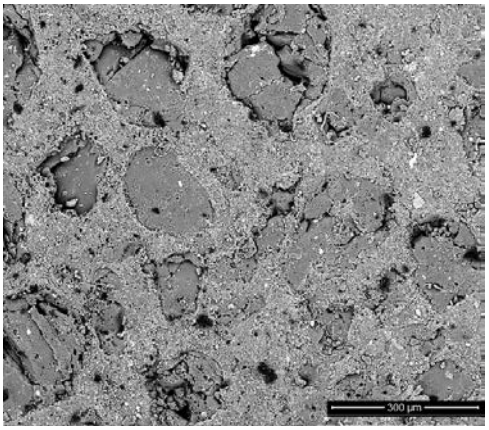

(a)

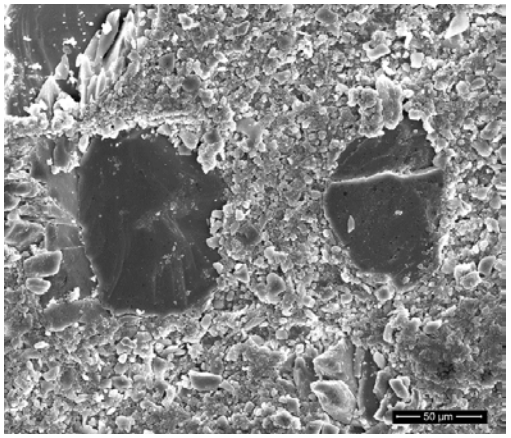

(b)

Figure 1: SEM micrograph of PBX

Modified SHPB setup

High rate uniaxial compression experiments are conducted on the PBX using a split Hopkinson pressure bar (SHPB) experiment. As shown in Fig. 2, a SHPB setup consists of a striker bar, an incident bar, and a transmission bar. A gas gun launches the striker bar at the incident bar and that impact causes an elastic compression wave to travel in the incident bar toward the specimen. When the impedance of the specimen is less than that of the bars, an elastic tensile wave will be reflected into the incident bar and an elastic compression then will be transmitted into the transmission bar. If the

elastic stress pulses in the bars are non-dispersive and the specimen deforms with homogeneous deformation, the elementary theory for wave propagation in bars can be used to calculate the sample response from measurements taken with strain gages mounted on the incident and transmission bars. The weak transmitted signal is very small, so the transmitted signal is measured by semiconductor strain gauge.

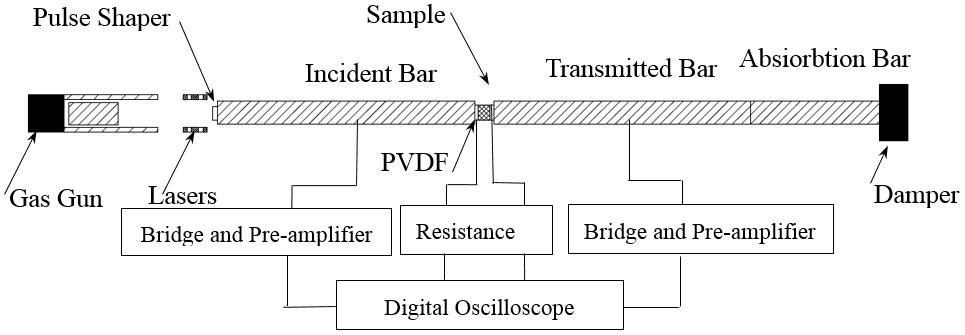

Figure 2: A schematic illustration of the pulse-shaped SHPB setup

The diameter of the striker, incident and transmission bars is 20 mm, and the length of the incident bar and transmission bars is 1500 mm. In our work, the bars are made of aluminum, of which density and Young's modulus are 2.7×10^3 kg/m^3 and 73 GPa, respectively. In order to minimize the effects of friction on specimen-bar interfaces, a thin layer of high-purity petroleum jelly is applied between the specimen and the bar ends.

Poly(vinylidene fluoride) (PVDF) gauges are used to measure the stress at the front and back face of specimen in this experiment [26, 27]. Quartz-crystal transducers have been used by investigators (Walley et al. [28-30]). However, the quartz-crystal transducers are very sensitive to test the environment, such as the environmental humidity, cleanliness, and the performance of the conductive adhesive, etc. The research showed that the piezoelectric PVDF as the transducers has the advantages of

high piezoelectric coefficient, high frequency response, and thin size. It is very suitable for measuring internal stress wave propagation in test material. The size of PVDF gauge is 8 mm × 8 mm × 100 μm.

There are two fundamental postulates for the current SHPB: the theory of one-dimensional elastic stress wave is valid in pressure bars, and the stress and strain states within the specimens are uniaxial and uniform. According to the conventional SHPB theory, the engineering strain rate $\dot{\varepsilon}(t)$, strain $\varepsilon(t)$ and stress $\sigma(t)$ in the specimen are calculated by

$$\dot{\varepsilon}(t) = -\frac{2c_0}{l_s}\varepsilon_r(t) \tag{1}$$

$$\varepsilon(t) = \int_0^t \dot{\varepsilon}(\tau)d\tau = \int_0^t \frac{2c_0}{l_s}\varepsilon_r(\tau)d\tau \tag{2}$$

$$\sigma(t) = \frac{A_0}{A_s}E\varepsilon_t(t) \tag{3}$$

where l_s and A_s are the original specimen length and cross-sectional area, respectively; E, c_0 and A_0 are the Young's modulus, elastic bar-wave velocity, and cross-sectional area of the bars, respectively; $\varepsilon_r(t)$ and $\varepsilon_t(t)$ are measured reflected and transmitted strain signals on the bar surfaces, respectively.

Size Thickness Effect

Size effect is the important factor that affects the stress uniformity in the specimens. Considering the matching size of specimen and bar, the ratio between the diameters is generally about 80%. When the lateral expansion of specimen is equal to the diameter of bar, axial strain can reach 30%. The aspect ratio of the specimens depends on the strain rate, the overall characteristics of the specimen size and two basic assumptions.

To determine the effect of specimen thickness on the dynamic stress-strain behavior of the PBX during a SHPB experiment, a series of tests are conducted on 16 mm diameter specimens with thicknesses of 4 mm, 3 mm and 2 mm. The striker initial velocity is adjusted by the gas gun pressure. Fig. 3 shows the incident, reflected and transmitted strain signals on SHPB without pulse shaper.

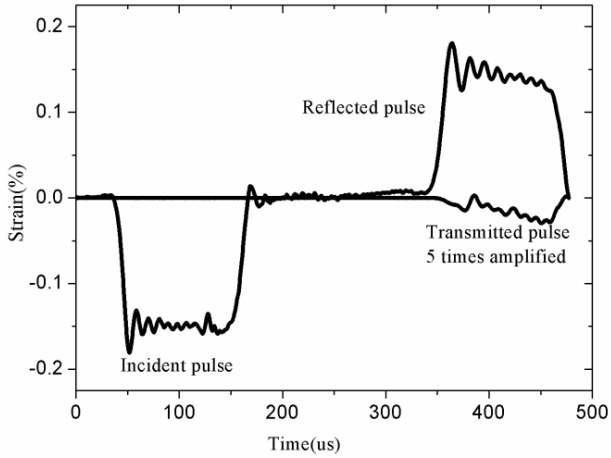

Figure 3: Oscilloscope records of a SHPB experiment with the specimen with thickness 4 mm without shaper pulse

Fig. 4(a) shows that the specimen with thickness 4 mm (aspect ratio of 0.25) is never in a state of dynamic stress equilibrium. Fig. 4(b) illustrates that the thickness is reduced to 3 mm, the back-end stress histories are getting close to the front-end stress histories, but the amplitude of the front-end stress is still significantly higher. When the thickness is reduced to 2 mm (aspect ratio of 0.125), there is a significant improvement in the stress uniformity is observed (Fig. 4(c)). However, the specimen thickness is very small, the stress uniformity of specimen can be grearly affected by the friction. The lateral deformation of the specimen is prevented by the friction, so the specimen presents bulge. As a result, the decrease of the specimen thickness

cannot be unlimited. The incident pulse needs to be controlled to avoid the sudden impact which results in the large spike in the front and back-end stress.

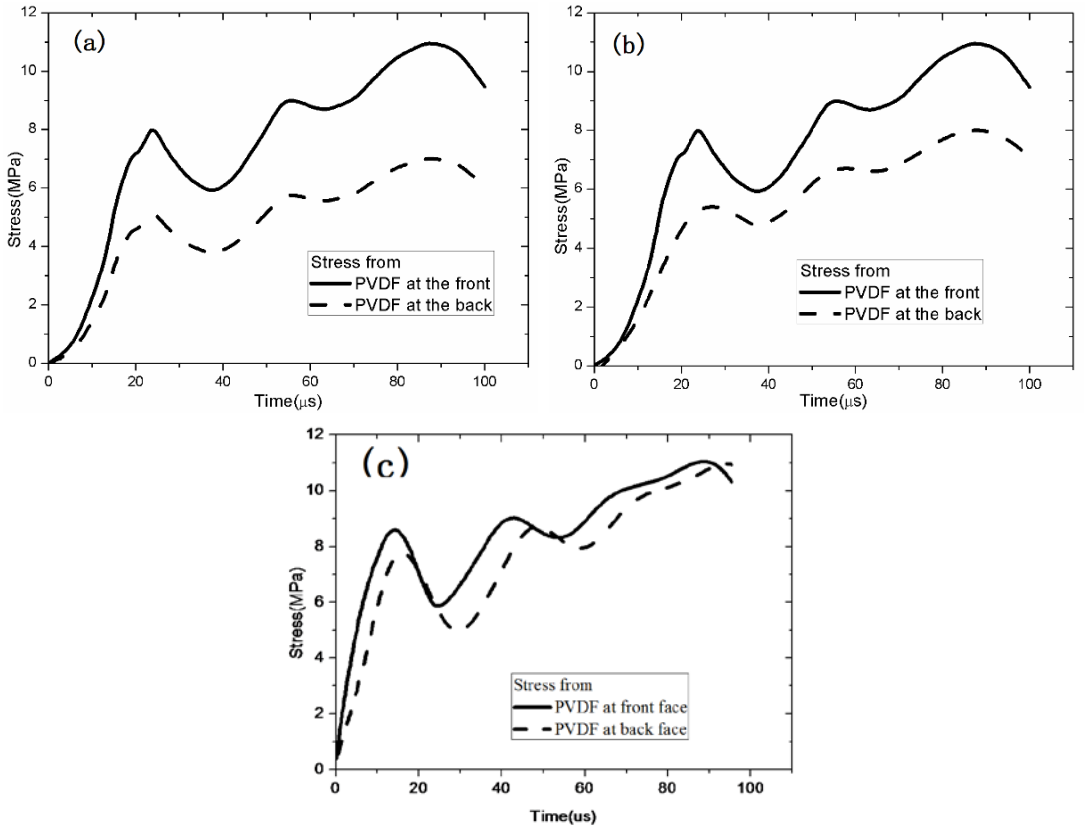

Figure 4: Front and back-end stress histories of binder during a SHPB test without pulse shaping for various thickness. (a) 4 mm, (b) 3 mm and (c) 2 mm.

Pulse Shaper

Pulse-shaping techniques, which employ a pulse shaper at the impact end of the incident bar, have been recently developed to generate an initially slow loading profile in the incident pulse so that the specimen can obtain the dynamic stress equilibrium in the elastic deformation stage. The dimensions and material of the pulse shaper can be properly determined to achieve the following conditions:

1. minimum dispersion effects

2. dynamic stress equilibrium

3. constant strain rate

To assist our experimental design procedures prior to testing, a model was developed to describe a general incident stress pulse. It is assumed that the state of specimen is one-dimensional stress. A ratio between the mechanical impedances of the specimen and the incident/transmitted bar is defined as $\beta = A\rho c / A_0\rho_0 c_0$, where ρ, c and A are the mass density, wave velocity and cross-sectional area of the specimen, respectively, and the subscript 0 represents for the incident/transmitted bar.

Following the propagation of stress wave, the stress in the specimen at left interface is

$$\sigma_1(t) = \frac{2\beta}{1+\beta}\sigma_i(t), \quad 0 \le t < 2\Delta t \tag{4}$$

$$\sigma_1(t) = \frac{2\beta}{1+\beta}\sigma_i(t) + \frac{2\beta}{1+\beta}\left[\left(\frac{1-\beta}{1+\beta}\right)^1 + \left(\frac{1-\beta}{1+\beta}\right)^2\right]\sigma_i(t-2\Delta t) + \cdots + \frac{2\beta}{1+\beta}\left[\left(\frac{1-\beta}{1+\beta}\right)^{k-1} + \left(\frac{1-\beta}{1+\beta}\right)^k\right]\sigma_i(t-k\Delta t), \quad k\Delta t \le t < (k+2)\Delta t \tag{5}$$

where k=2n, (n=1, 2, 3…).

The stress at right interface is

$$\sigma_2(t) = 0, \quad 0 \le t < \Delta t \tag{6}$$

$$\sigma_2(t) = \frac{2\beta}{1+\beta}\left[1 + \left(\frac{1-\beta}{1+\beta}\right)\right]\sigma_i(t-3\Delta t) + \cdots + \frac{2\beta}{1+\beta}\left[\left(\frac{1-\beta}{1+\beta}\right)^{k-1} + \left(\frac{1-\beta}{1+\beta}\right)^k\right]\sigma_i(t-k\Delta t), \quad k\Delta t \le t < (k+2)\Delta t \tag{7}$$

where k=2n-1, (n=1, 2, 3…).

The pulse has a rising edge in the form of a linear ramp with a finite rise time τ_0. The degree of stress uniformity can be quantified by the parameter α_k in the

specimen, defined by $\alpha_k = \Delta\sigma_k / \sigma_k$, where the stress increment is $\Delta\sigma_k = \sigma_k - \sigma_{k\text{-}1}$, describing the change in the specimen after the incident wave has propagated *k* times from one end of the specimen to the other. It is defined that $\alpha_k \leq 5\%$, for the stress to be uniform in the specimen (also shown by Ravichandran and Subhask in 1994 [31]).

The ratio of mechanical impedance of the specimen of PBX and the incident/transmitted bar is $\beta = 1/25$. The different ramp rise time τ_0 on the degree of stress uniformity is plotted in Fig. 5. Table 1 shows how the number of required wave transits *n* varies with the ramp rising time τ_0, when $\beta = 1/25$.

In this study, the pulse shapers were made of different materials, such as lead, rubber and copper. Through theoretic prediction and trial experiment, lead disks with diameter of 6.5 mm and thickness of 1.3 mm were selected as the pulse shaper. The rise time of the incident wave is 40 μs. After incident wave transits 5 or 4 times, specimen can achieve stress uniformity and obtain a constant strain rate.

Fig. 6 shows the oscilloscope records of the incident $\varepsilon_i(t)$, reflected $\varepsilon_r(t)$ and transmitted strain $\varepsilon_t(t)$ signals on the pulse-shaped SHPB. Here, point A to B, as the nearly flat plateau, indicates that the specimen deformed at a nearly constant strain rate. Fig. 7 shows the front and back stress histories during a SHPB test with pulse shaping thickness of 2 mm, and the front-end stress history is consistent with the back-end stress history. The specimen can obtain the sterss uniformity in current SHPB tests. Fig. 8(a) shows a typical dynamic strain history of the PBX specimen at average strain rate of 2000 s^{-1}. Here, point A and B correspond to A and B in the Fig. 6, and AB, as

linear function, illustrates the nearly constant strain rate. The average strain rate can be calculated over 50 μs to 130 μs. At 130 μs, the sample unloads and recovers intact.

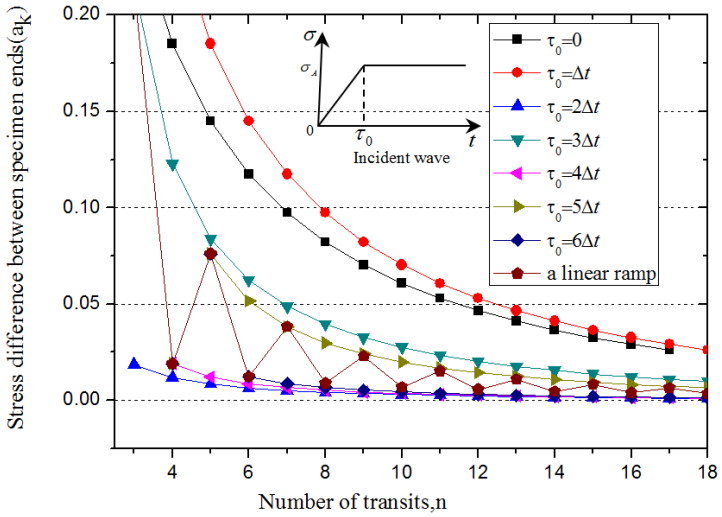

Figure 5: Under different incident waves, variation of stress uniformity with number of wave transits for bar–specimen relative impedances (β=1/25).

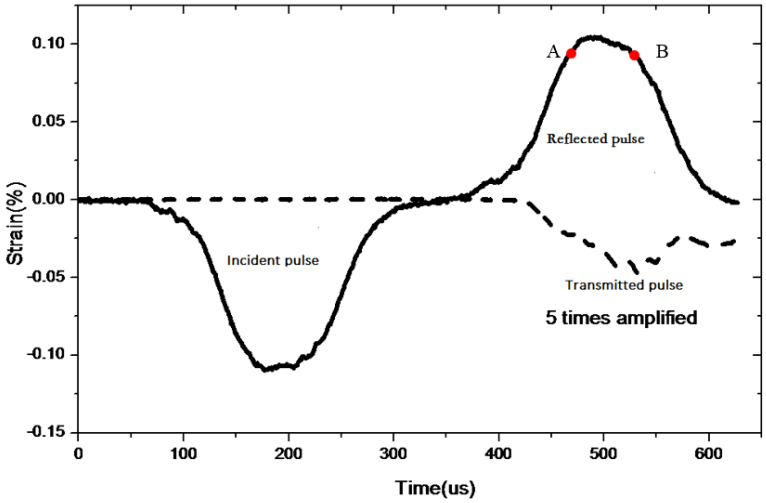

Figure 6: Typical incident, reflected, and transmitted waves from a pulse-shaped experiment with a SHPB modified for PBX testing.

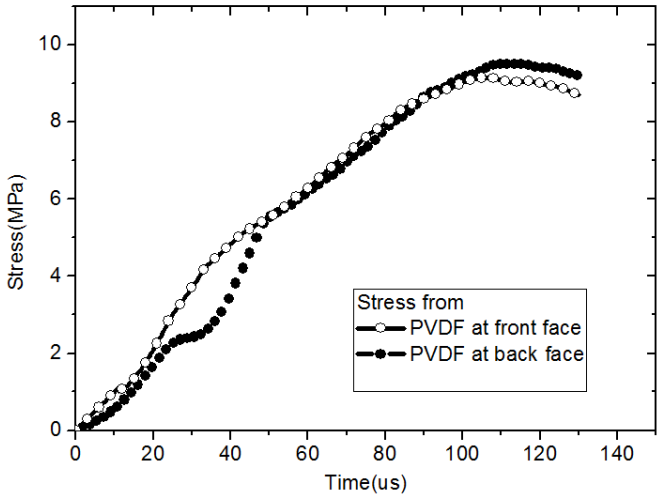

Figure 7: A comparison of the axial forces on the front- and back- end of a PBX specimen

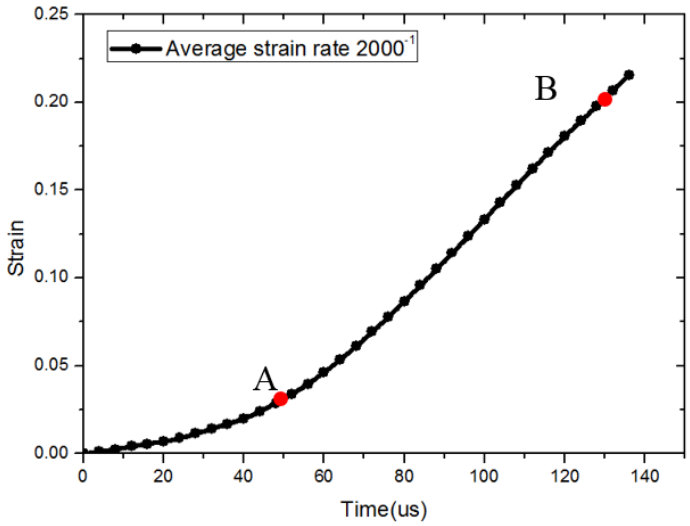

Figure 8: A typical dynamic strain history of a PBX specimen

Using such smooth bar end-faces and proper lubrication in the dynamic experiments, the thin specimen expands in radial directions nearly freely as shown in the high-speed digital images in Fig. 9, which were taken using back-light illumination condition to show the specimen edge more clearly. It is also can be observed in Fig. 9 also shows that the specimen deformed uniformly.

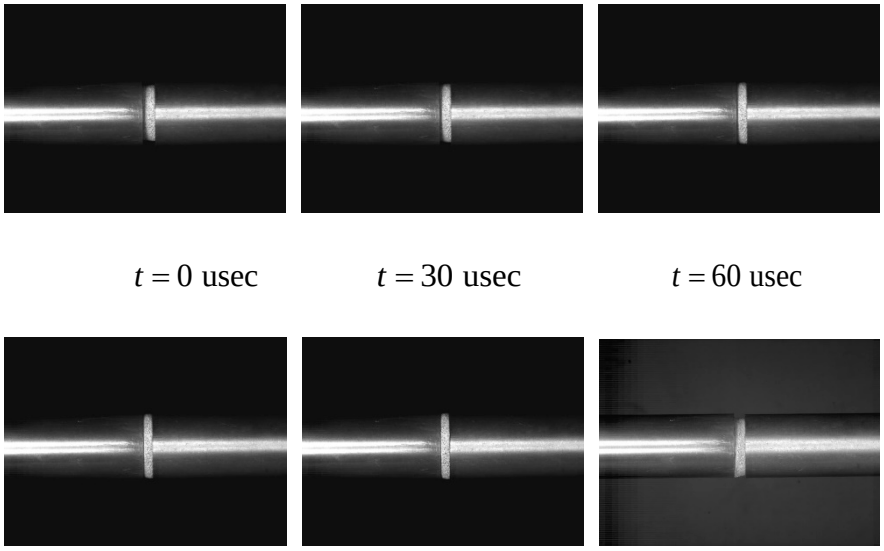

Figure 9: High-speed deformation of a PBX sample under dynamic compressive test

Experimental results

Fig. 10 shows that the damaged PBX specimens after SHPB tests. It can be observed that the specimens are not obviously damaged at the strain rate of 1292 s^{-1}, and at the strain rate of 2000 s^{-1} the specimens are obviously damaged. Fig. 10(b) shows the macroscopic radial and circumferential cracks caused by a mechanical impact at the strain rate of 2000 s^{-1}. The most noticeable feature in these figures is the change in Young's modulus, at low strains, as the rate changes. These changes come entirely from the viscoelastic binder since the crack growth is not significant at low strains.

A number of the SHPB tests are conducted on the PBX specimens. Fig. 11 shows the stress-strain curves of PBX specimens at strain rates of 891 s^{-1}, 1292 s^{-1} and 2000 s^{-1}, respectively. Because the length of striker is 150 mm, the effective load time is

about 110 μs. It can be observed that the specimens do not obviously damage at the strain rate of 891 s^{-1} and 1292 s^{-1}. The individual plots with either an "X" or "O" states whether the specimen has failed or not failed, respectively. The "failed" compression test specimens are confirmed by the visible cracks. As a result, the PBX specimens tested at 2000 s^{-1} and higher strain rate have various cracks in the direction of loading.

Figure 10: The PBX samples recovered. (a) The strain rate 1292 s^{-1}; (b) the strain rate 2000 s^{-1}

The compressive stress-strain curves of PBX were found to be dependent on the strain rate. The compressive strength rises with the increasing strain rate, and the shape of the stress-strain curves for the five sets of specimens are identical. Increasing the strain rate leads to high moduli owing to the polymer chains has reduced relaxation time. These measurements provide the basis to develop and validate predictive material strength models for PBX. The maximum flow stress of PBX is 19 MPa, and the strain-at-maximum stress value is 0.22 at the strain rate of 2000 s^{-1}.

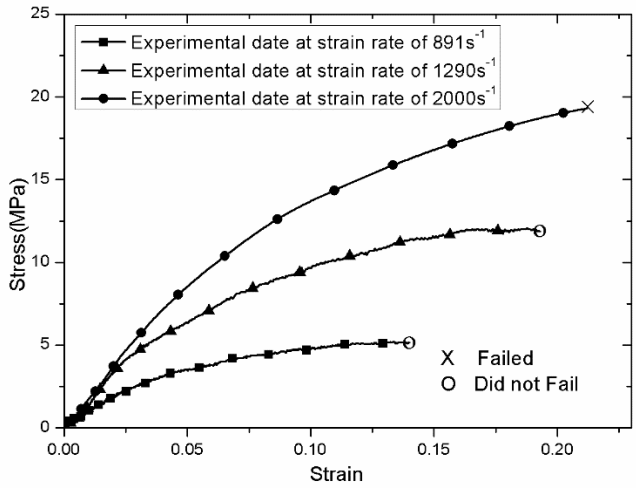

Figure 11: Dynamic compressive stress-strain curves of PBX on different strain rates

Constitutive Equation with Strain Rate Effects

A strain-energy function approach was developed to accurately describe the dynamic compressive behavior of the PBX. The PBX is an isotropic incompressible solid. The strain-energy function U can be written as [32]

$$U = \sum_{i=0,i=0}^{n} C_{ij}(I_1 - 3)^i (I_2 - 3)^j \tag{8}$$

where C_{ij} is polynomial coefficient, i and j are polynomial powers, I_1 and I_2 are strain invariants.

$$I_1 = \lambda^2 + \frac{2}{\lambda} \tag{9}$$

$$I_2 = \frac{1}{\lambda^2} + 2\lambda \tag{10}$$

where λ is the stretch ratio.

The first-order relation for strain-energy is

$$U = C_1(I_1 - 3) + C_2(I_2 - 3) \tag{11}$$

Experimental results present the complicated stress-strain curves. The strain-energy

function was given as

$$U = C_1(I_1 - 3) + C_2(I_2 - 3) + C_3(I_2 - 3)^2 \tag{12}$$

where C_1, C_2, and C_3 are constant polynomial coefficients. In order to apply Eq. 12 to our uniaxial loading experiments, the stretch ratios were given as

$$\lambda_1 = \lambda \tag{13}$$

$$\lambda_2 = \lambda_3 = \lambda^{-1/2} \tag{14}$$

where λ is the stretch in the loading direction, and

$$\lambda = 1 - \varepsilon_E \tag{15}$$

where ε_E is the engineering strain for uniaxial compression.

With the assumption of incompressible volume to simplify the constitutive model, the constitutive relation can be formulated as follows

$$\sigma_{sef} = 2\left(\lambda^2 - \frac{1}{\lambda}\right)\left(\frac{\partial U}{\partial I_1} + \frac{1}{\lambda}\frac{\partial U}{\partial I_2}\right) \tag{16}$$

where σ_{sef} is the ture stress in the material.

Substitution of Eq. (12) into (16) lead to

$$\sigma_{sef} = 2\left(\lambda^2 - \frac{1}{\lambda}\right)\left(A_1 + A_2\frac{1}{\lambda} + A_3\frac{1}{\lambda^3}\right) \tag{17}$$

where A_1, A_2 , and A_3 are combinations of C_1 , C_2 , and C_3

$$\begin{cases} A_1 = C_1 + 4C_3 \\ A_2 = C_2 - 6C_3 \\ A_3 = C_3 \end{cases} \tag{18}$$

The strain rate effects need to be considered. The following model was therefore developed to accurately describe the strain-rate effects on the dynamic properties of the PBX

$$\sigma = \sigma_{sef}\left[\left(\frac{1}{\lambda}\right)^{-\beta \lg \dot{\varepsilon}/\dot{\varepsilon}_0} + \left(\frac{1}{\lambda}\right)^{-N_1}\frac{N_2}{1+N_3 \lg \dot{\varepsilon}/\dot{\varepsilon}_0}\right] \tag{19}$$

Substitution of Eq. (17) into (19) lead to

$$\sigma = 2\left(\lambda^2 - \frac{1}{\lambda}\right)\left(A_1 + A_2\frac{1}{\lambda} + A_3\frac{1}{\lambda^3}\right)\left[\left(\frac{1}{\lambda}\right)^{-\beta \lg \dot{\varepsilon}/\dot{\varepsilon}_0} + \left(\frac{1}{\lambda}\right)^{-N_1}\frac{N_2}{1+N_3 \lg \dot{\varepsilon}/\dot{\varepsilon}_0}\right] \tag{20}$$

where $\dot{\varepsilon}_0$ is the reference strain rate, and β is material constants, the numerical values of which are listed in Table 1 for the PBX.

Table 1 Material constants for the constitutive model

A_1/MPa	A_2/MPa	A_3/MPa	N_1	N_2	N_3	β	$\dot{\varepsilon}_0$/s^{-1}
-17.8681	-4.8947	0.077	22.5	6.5	-9.5	-5.1962	5000^{-1}

The comparisons of the predicted and experimental uniaxial stress-strain curves at strain rate of 890 s^{-1}, 1290 s^{-1}, and 2000 s^{-1} are shown in Fig. 12. In general, Fig. 12 illustrates the predicted stress responses are in good agreement with the measured ones.

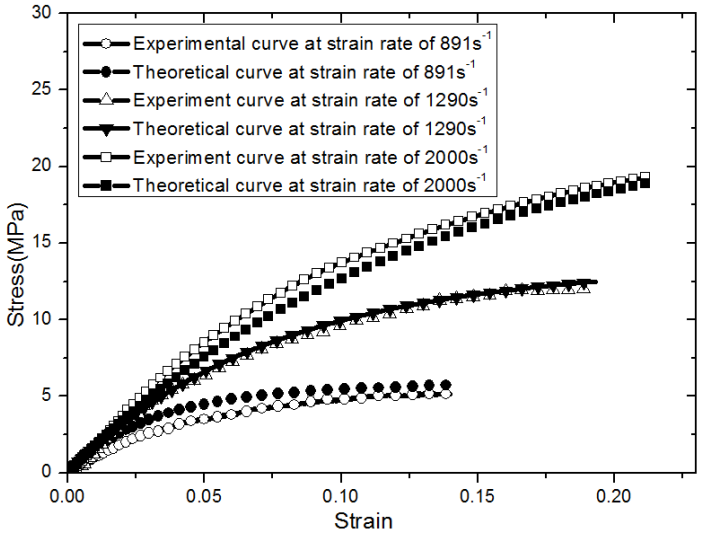

Figure 12: Comparison of theoretical and experimental uniaxial dynamic compressive stress-strain curves of PBX

Conclusions

The methodologies to obtain the dynamic properties of PBX are systematically discussed in detail. In order to obtain valid data, the thickness of the specimen and the shape of the incident wave are designed to make sure that the specimens are in dynamic stress uniformity and deform homogeneously at a nearly constant strain rate. Reducing the thickness alone cannot achieve dynamic stress equilibrium and homogeneous deformation in the soft specimen. The loading pulse profile must also be carefully shaped using a pulse-shaping technique to ensure a homogeneous deformation at a constant strain rate in thin specimens during dynamic experiments. Based on the experimental results, a constitutive model is adequate to account for the dynamic mechanical behavior of high binder content PBXs.

Acknowledgments

The present work was supported by the Aerospace Science and Technology Innovation Fund Projects of Harbin Institute of Technology (CASA-HIT12-1A02).

References

[1] Chen P., Xie H., Huang F., Huang T., and Ding Y. (2006) Deformation and failure of polymer bonded explosives under diametric compression test. *Polym. Test*. **25**. 333–341.

[2] Chen P., Huang F., and Ding Y. (2007) Microstructure, deformation and failure of polymer bonded explosives. *J Mater Sci* **42**. 5272-5280.

[3] Xiao Y., Sun Y., Zhen Y., Guo L., and Yao L. (2017) Characterization, modeling and simulation of the impact damage for polymer bonded explosives. *Int. J. Impact Eng* **103**. 149-158.

[4] Xiao Y. C., Sun Y., Li X., Zhang Q. H., Liu S. W., and Yang H. (2016) Dynamic Mechanical Behavior of PBX. *Propellants Explosives Pyrotechnics* **41**. 629-636.

[5] Xiao Y., Sun Y., Yang Z., and Guo L. (2017) Study of the dynamic mechanical behavior of PBX by Eshelby theory Acta Mechanica. (Online)

[6] Xiao Y., Sun Y., Yang Z., and Guo L. (2017) Dynamic Compressive Properties of Polymer Bonded Explosives under Confining Pressure. *Propellants Explosives*

*Pyrotechnics. (*Published*)*

[7] Idar D., Thompson D., Gray G., Blumenthal W., Cady C., Peterson P., Roemer E., Wright W., and Jacquez B. (2002) Influence of polymer molecular weight, temperature, and strain rate on the mechanical properties of PBX 9501 *in Aip conference proceedings*, 821-824.

[8] Funk D. J., Laabs G. W., Peterson P. D., and Asay B. W. (1996) Measurement of the stress/strain response of energetic materials as a function of strain rate and temperature: PBX 9501 and mock 9501 *in Proceedings of the conference of the American Physical Society topical group on shock compression of condensed matter*, 145-148.

[9] Blumenthal W., Gray III G., Idar D., Holmes M., Scott P., Cady C., and Cannon D. (2000) Influence of temperature and strain rate on the mechanical behavior of PBX 9502 and Kel-F 800™ *in SHOCK COMPRESSION OF CONDENSED MATTER-1999*, 671-674.

[10] Colak O. U. (2004) Mechanical Behavior of PBXW-128 and PBXN-110 under Uniaxial and Multiaxial Compression at Different Strain Rates and Temperatures. *Turkish Journal of Engineering & Environmental Sciences*

[11] Kolsky H. (1949) An investigation of the mechanical properties of materials at very high rates of loading. *Proc. Phys. Soc. London, Sect. B* **62**. 676.

[12] Chen W., Song B., Frew D., and Forrestal M. (2003) Dynamic small strain measurements of a metal specimen with a split Hopkinson pressure bar. *Exp. Mech.* **43**. 20-23.

[13] Chen W., Zhang B., and Forrestal M. (1999) A split Hopkinson bar technique for low-impedance materials. *Exp. Mech.* **39**. 81-85.

[14] Song B. and Chen W. (2004) Loading and unloading split Hopkinson pressure bar pulse-shaping techniques for dynamic hysteretic loops. *Exp. Mech.* **44**. 622-627.

[15] Song B. and Chen W. (2004) Dynamic stress equilibration in split Hopkinson pressure bar tests on soft materials. *Exp. Mech.* **44**. 300-312.

[16] Song B., Chen W., Ge Y., and Weerasooriya T. (2007) Dynamic and quasi-static compressive response of porcine muscle. *J. Biomech.* **40**. 2999-3005.

[17] Song B., Chen W., and Weerasooriya T. (2003) Quasi-Static and Dynamic Compressive Behaviors of a S-2 Glass/SC15 Composite. *J. Compos. Mater.* **37**. 1723-1743.

[18] Chen W., Lu F., Frew D., and Forrestal M. (2002) Dynamic compression testing of soft materials. *J. Appl. Mech.* **69**. 214-223.

[19] Frew D., Forrestal M. J., and Chen W. (2001) A split Hopkinson pressure bar technique to determine compressive stress-strain data for rock materials. *Exp. Mech.* **41**. 40-46.

[20] Frew D., Forrestal M. J., and Chen W. (2002) Pulse shaping techniques for testing brittle materials with a split Hopkinson pressure bar. *Exp. Mech.* **42**. 93-106.

[21] Follansbee P. and Kocks U. (1988) A constitutive description of the deformation of copper based on the use of the mechanical threshold stress as an internal state

variable. *Acta Metall.* **36**. 81-93.
[22] Duffy J., Campbell J. D., and Hawley R. H. (1971) On the Use of a Torsional Split Hopkinson Bar to Study Rate Effects in 1100-0 Aluminum. *J. Appl. Mech.* **38**. 83-91.
[23] Swanson S. and Christensen L. (1983) A constitutive formulation for high-elongation propellants. *Journal of Spacecraft and Rockets* **20**. 559-566.
[24] Park S. and Schapery R. (1997) A viscoelastic constitutive model for particulate composites with growing damage. *Int. J. Solids Struct.* **34**. 931-947.
[25] Mas E. M., Clements B. E., Blumenthal W. R., Cady C. M., Gray G. T., and Liu C. (2002) A viscoelastic model for PBX binders in *Shock Compression of Condensed Matter-2001, Pts 1 and 2, Proceedings*. vol. 620, M. D. Furnish, N. N. Thadhani, and Y. Horie, Eds., 661-664.
[26] Wang Y.-C. and Chen Y.-W. (2007) Application of piezoelectric PVDF film to the measurement of impulsive forces generated by cavitation bubble collapse near a solid boundary. *Exp. Therm Fluid Sci.* **32**. 403-414.
[27] Zeng F.-l., Sun Y., Zhou Y., and Li Q.-k. (2011) A molecular dynamics simulation study to investigate the elastic properties of PVDF and POSS nanocomposites. *Modell. Simul. Mater. Sci. Eng.* **19**. 025005.
[28] Field J., Walley S., Proud W., Goldrein H., and Siviour C. (2004) Review of experimental techniques for high rate deformation and shock studies. *Int. J. Impact Eng* **30**. 725-775.
[29] Walley S. M., Field J. E., Pope P. H., and Safford N. A. (1989) A Study of the Rapid Deformation Behaviour of a Range of Polymers. *Philosophical Transactions of the Royal Society A: Mathematical, Physical and Engineering Sciences* 1-33.
[30] Siviour C. R., Walley S. M., Proud W. G., and Field J. E. (2005) The high strain rate compressive behaviour of polycarbonate and polyvinylidene difluoride. *Polymer* **46**. 12546-12555.
[31] Ravichandran G. and Subhash G. (1994) Critical appraisal of limiting strain rates for compression testing of ceramics in a split Hopkinson pressure bar. *J. Am. Ceram. Soc.* **77**. 263-267.
[32] Han C. D. (1985) Mechanical properties of solid polymers, 2nd ed., I. M. Ward, Wiley, New York, 1983, 475 pp. Price: $54.95. *Journal of Polymer Science Polymer Letters Edition* **23**. 119-119.